Available online at www.sciencedirect.com
ScienceDirect
Journal of Solid State Chemistry 180 (2007) 1193–1197
JOURNAL OF SOLID STATE CHEMISTRY
www.elsevier.com/locate/jssc

Structure and antiferroelectric properties of cesium niobate, $Cs_2Nb_4O_{11}$

Robert W. Smith[a,*], Chunhua Hu[b], Jianjun Liu[c], Wai-Ning Mei[c], Kuan-Jiuh Lin[d]

[a]*Department of Chemistry, University of Nebraska at Omaha, Omaha, NE 68182, USA*
[b]*Nebraska Center for Materials and Nanoscience, University of Nebraska–Lincoln, Lincoln, NE 68588, USA*
[c]*Department of Physics, University of Nebraska at Omaha, Omaha, NE 68182, USA*
[d]*Department of Chemistry, Center of Nanoscience and Nanotechnology, National Chung-Hsing University, Taichung 402, Taiwan, Republic of China*

Received 8 November 2006; received in revised form 12 January 2007; accepted 14 January 2007
Available online 26 January 2007

Abstract

The compound cesium niobate, $Cs_2Nb_4O_{11}$, is an antiferroelectric, as demonstrated by double hysteresis loops in the electric field versus polarization plot. The crystal structure refinement by X-ray diffraction at both 100 and 297 K shows it to have a centrosymmetric structure in point group *mmm* and orthorhombic space group *Pnna*, which is consistent with its antiferroelectric behavior. The 100-K structure data is reported herein. The lattice is comprised of niobium-centered tetrahedra and octahedra connected through shared vertices and edges; cesium atoms occupy channels afforded by the three-dimensional polyhedral network. Antiferroelectricity is produced by antiparallel displacements of niobium atoms along the *c*-axis at the phase transition temperature of 165 °C. The critical field for onset of ferroelectric behavior in a single-crystal sample is 9.5 kV/cm at room temperature.

Keywords: Structure; X-ray diffraction; Antiferroelectricity

1. Introduction

Cesium niobate (or CNO), which has the chemical formula $Cs_2Nb_4O_{11}$, was first reported as a component of the Cs_2O/Nb_2O_5 phase diagram by Reisman and Mineo [1] in 1961, and the crystal structure was subsequently refined in the polar point group *mm*2 and noncentrosymmetric space group *Pnn*2 by Gasperin [2] in 1981. Kharitonova et al. [3] studied its physical properties and reported it to have a ferroelectric-type phase transition at 164 °C with little temperature hysteresis, from which they surmised the transition to be second order. It has also recently been reported to be a photocatalyst for the decomposition of water [4].

As part of our on-going investigation into ferroelectrics and high-dielectric materials, we embarked on a project to further investigate the reported ferroelectric transition and explain its origin. In the course of this project, we confirmed the transition at 165 °C from the temperature dependence of complex capacitance, impedance, and polarized Raman spectra of a single-crystal sample [5]. Upon examination of the room-temperature hysteresis, however, we were surprised to observe the double hysteresis loop of an antiferroelectric rather than the single loop of a ferroelectric material.

Ferroelectricity requires a noncentrosymmetric structure in a polar point group, but antiferroelectricity requires a nonpolar point group [6]. The reported structure of CNO in space group *Pnn*2 (and polar point group *mm*2) would therefore be incorrect if CNO were antiferroelectric.

Because of these conflicting results, we sought to resolve the matter by conducting a second harmonic generation (or SHG) experiment. A second harmonic can only be produced from noncentrosymmetric materials and can be viewed as a necessary result of such materials. An 800-nm laser beam was passed through the CNO crystal, and the 400-nm SHG signal was monitored with a spectrometer equipped with an 800-nm filter. A β-BaB_2O_4 crystal was used to optimize the optical path. We detected no 400-nm output from the CNO crystal, which put its reported structure in question. We consequently decided to determine the space group and crystal structure through our own single-crystal refinement, which is reported herein with

*Corresponding author. Fax: +1 402 554 3888.
E-mail address: robertsmith@mail.unomaha.edu (R.W. Smith).

0022-4596/$ - see front matter © 2007 Elsevier Inc. All rights reserved.
doi:10.1016/j.jssc.2007.01.015

the antiferroelectric hysteresis results and an analysis of the atomic displacements that produce the effect. Crystal structure refinement at 100 K and room temperature showed the material to be in the nonpolar point group *mmm* and space group *Pnna*.

2. Experimental

2.1. X-ray diffraction and structure refinement

Large single crystals of CNO were grown from the binary system using the flux method, the details of which have been described elsewhere [3]. From a larger crystal mass, we cut a block-shaped single crystal with dimensions $0.07 \times 0.12 \times 0.17$ mm and mounted it on a 20-μm Hampton CryoLoops for subsequent X-ray diffraction data collection. Geometry and intensity data were obtained at 100 K and 297 K on a Bruker diffractometer equipped with a SMART Apex CCD area detector and Oxford Cryosystems 700 cooler [7]. Both data sets yielded the same results, and only the 100-K data and refinement are reported herein. Radiation was monochromatic Mo$K\alpha$ ($\lambda = 0.71073$ Å). Data were collected with the ω-scan method.

Data were processed with the SAINT + program [8] for reduction and cell refinement. Multi-scan absorption corrections were applied to the data sets by the SADABS program [9]. The structure was solved by direct methods and refined using SHELXTL [10]. Systematic absences (including that for the a-glide) unambiguously indicated space group *Pnna*. All atoms were refined with anisotropic displacement parameters. Crystal data and refinement results are listed in Table 1. Further details of the crystal structure investigation can be obtained from the Fachinformationszentrum Karlsruhe, 76344 Eggenstein–Leopoldshafen, Germany, (fax: +49 7247 808 666; e-mail: crysdata@fiz.karlsruhe.de) on quoting the depository numbers CSD 417408 and 417409 for the 100-K and 297-K data, respectively.

2.2. Ferroelectric hysteresis

Electric-field dependence of polarization was measured with a Radiant Technology Precision LC ferroelectric tester with a Trek signal amplifier. Gold films were sputtered on a 4-mm thick single crystal as electrodes on both faces normal to the *c*-axis, which is the axis along which high-field polarization occurs. The crystal faces were indexed from a combination of crystal morphology, X-ray diffraction, and polarization microscopy. The electric field applied was −12.5 to 12.5 kV/cm and 1 Hz.

3. Results

Atomic coordinates and isotropic thermal coefficients for the 100-K refinement are shown in Table 2. A view of the structure is shown in Fig. 1.

Table 1
Crystallographic data for $Cs_2Nb_4O_{11}$

Formula mass (amu)	813.46
Space group	*Pnna* (No. 52)
a (Å)	7.46660(10)
b (Å)	28.9047(4)
c (Å)	10.48570(10)
V (Å^3)	2263.02(5)
Z	8
ρ_{calcd} (g cm^{-3})	4.775
Temperature (K)	100(2)
Crystal dimensions (mm)	$0.16 \times 0.12 \times 0.07$
Radiation	Graphite monochromated Mo$K\alpha$, $\lambda = 0.71073$ Å
μ(Mo$K\alpha$) (mm^{-1})	10.336
Transmission factors	0.2886–0.5315
2θ limits	$2.82^\circ \leqslant 2\theta(\text{Mo}K\alpha) \leqslant 55.98^\circ$
Data collected	$-9 < h < 9$, $-38 < k < 38$, $-13 < l < 13$
No. of data collected	28,176
No. of unique data	2728
R_{int}	0.0300
No. of variables	156
$R(F)$ for $F_o^2 > 2\sigma(F_o^2)$	0.0172
$R_w(F_o^2)$	0.0473
Goodness of fit	1.118
$(\Delta\rho)_{max}$, $(\Delta\rho)_{min}$ (e Å^{-3})	0.941, −0.849

Table 2
Atomic coordinates and equivalent isotropic displacement parameters for $Cs_2Nb_4O_{11}$

Atom	Wyckoff position	*x*	*y*	*z*	U_{eq} (Å^2)[a]
Cs(1)	8*e*	0.7552(1)	0.1924(1)	0.1230(1)	0.014(1)
Cs(2)	8*e*	0.7522(1)	0.0756(1)	0.3535(1)	0.010(1)
Nb(1)	4*c*	$\frac{1}{4}$	0	0.2312(1)	0.005(1)
Nb(2)	4*d*	0.2401(1)	$\frac{1}{4}$	$\frac{1}{4}$	0.006(1)
Nb(3)	8*e*	0.2455(1)	0.1253(1)	0.2613(1)	0.005(1)
Nb(4)	8*e*	0.5015(1)	0.0613(1)	0.0018(1)	0.005(1)
Nb(5)	8*e*	0.5164(1)	0.1883(1)	0.4887(1)	0.005(1)
O(1)	8*e*	0.0615(3)	0.0998(1)	0.1335(2)	0.008(1)
O(2)	8*e*	0.0650(3)	0.1368(1)	0.3778(2)	0.007(1)
O(3)	8*e*	0.0645(3)	0.2335(1)	0.3749(2)	0.007(1)
O(4)	8*e*	0.2493(2)	0.0517(1)	0.3298(2)	0.007(1)
O(5)	8*e*	0.2481(2)	0.1844(1)	0.1859(2)	0.007(1)
O(6)	8*e*	0.4525(3)	0.0002(1)	0.1241(2)	0.006(1)
O(7)	8*e*	0.4392(3)	0.1002(1)	0.1330(2)	0.008(1)
O(8)	8*e*	0.4362(3)	0.1365(1)	0.3761(2)	0.007(1)
O(9)	8*e*	0.4365(3)	0.2340(1)	0.3727(2)	0.007(1)
O(10)	8*e*	0.7508(2)	0.0529(1)	0.0514(2)	0.008(1)
O(11)	8*e*	0.7529(2)	0.1854(1)	0.4352(2)	0.007(1)

[a] U_{eq} is defined as one-third of the trace of the orthogonalized U_{ij} tensor.

The structural motif of CNO in our refinement is very similar to that reported in Ref. [2], though in a different space group, so only a brief discription is necessary. The structure is a three-dimensional network of niobium-centered tetrahedra and octahedra connected through shared vertices and edges. The network is built from chains of vertex-connected octahedra and tetrahedra that

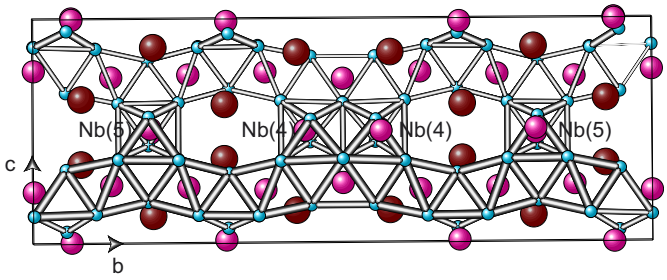

Fig. 1. View of the CNO structure along the *a*-axis. Large atoms are Cs, small atoms are O.

run parallel to the *b*-axis. The sequence of polyhedra is three octahedra followed by a tetrahedron. These chains connect parallel to the *c*-axis by shared vertices with Nb(4) and Nb(5)-centered octahedra, pairs of the former being connected to each other through shared edges. Cesium atoms occupy channels afforded by the polyhedral network. As shall be discussed below, the antiferroelectric properties of CNO are caused by the distortion of the Nb(4) and Nb(5)-centered octahedra and the displacement of the Nb atoms contained therein upon passage through the phase transition at 165 °C.

Average tetrahedral Nb–O bond distances are 1.85 ± 0.04 Å, and average octahedral Nb–O bond distances are 2.00 ± 0.12 Å. These values compare well with the expected values of 1.88 and 2.04 Å, respectively, derived from the ionic radii reported by Shannon [11]. Though not unprecedented, four-coordinate Nb^{5+} is rare, since the cation is usually too large to occupy a tetrahedron afforded by oxide anions. Reported tetrahedral niobates include the rare-earth niobates $ANbO_4$ (A = La, Nd, Ho, and Yb) [12]. In these compounds, the average Nb–O bond distance is 1.834 Å, which also compares well with our value. The niobium-centered polyhedra in our structure are also fairly regular: tetrahedral bond angles range from 106.8° to 110.6°, and octahedral bond angles for adjacent oxygen atoms range from 74.6° to 105.5°, with most within a few degrees of the ideal.

The cesium atoms are twelve and ten-coordinate with average Cs–O bond distances of 3.50 ± 0.22 Å and 3.35 ± 0.27 Å, respectively. These are slightly larger than the expected values of 3.28 and 3.21 Å, which are also derived from Shannon. Table 3 lists some selected bond distances and angles.

Fig. 2 displays the electric-field dependence of polarization at room temperature for CNO. It clearly exhibits double hysteresis loops, which are the basic characteristics of an antiferroelectric material. Generally, an antiferroelectric crystal has a zero net switchable dipole moment due to the antiparallel alignment of elementary dipoles in its unit cell [13]. When the external electric field is weak, the induced polarization is proportional to the field and exhibits no macroscopic polarization hysteresis. When the electric field exceeds a threshold value, called the critical field, the crystal becomes ferroelectric and the polarization

Table 3
Selected bond distances and angles for $Cs_2Nb_4O_{11}$

Bond	Distance (Å)	Bond	Distance (Å)
Nb(1)–O(4)	1.817(2) × 2	Nb(4)–O(1)	1.858(2)
Nb(1)–O(6)	1.884(2) × 2	Nb(4)–O(6)	2.214(2)
⟨Nb(1)–O⟩	1.85 ± 0.04	Nb(4)–O(6)	2.240(2)
Nb(2)–O(3)	1.913(2) × 2	Nb(4)–O(7)	1.837(2)
Nb(2)–O(5)	2.013(2) × 2	Nb(4)–O(10)	1.948(2)
Nb(2)–O(9)	2.005(2) × 2	Nb(4)–O(10)	1.968(2)
⟨Nb(2)–O⟩	1.98 ± 0.05	⟨Nb(4)–O⟩	2.01 ± 0.18
Nb(3)–O(1)	2.056(2)	Nb(5)–O(1)	2.074(2)
Nb(3)–O(2)	1.849(2)	Nb(5)–O(1)	1.971(2)
Nb(3)–O(4)	2.247(2)	Nb(5)–O(1)	1.998(2)
Nb(3)–O(5)	1.881(2)	Nb(5)–O(1)	1.892(2)
Nb(3)–O(7)	2.105(2)	Nb(5)–O(1)	1.855(2)
Nb(3)–O(8)	1.892(2)	Nb(5)–O(1)	2.125(2)
⟨Nb(3)–O⟩	2.01 ± 0.16	⟨Nb(5)–O⟩	1.96 ± 0.10
Bonds	Angle (°)		
O(4)–Nb(1)–O(4)	110.62(13)		
O(4)–Nb(1)–O(6)	109.83(8) × 4		
O(6)–Nb(1)–O(6)	106.81(13)		

⟨ ⟩ Indicates the average bond length.

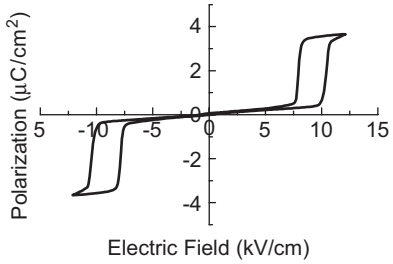

Fig. 2. Electric-field dependence of polarization for CNO at room temperature.

displays hysteresis with respect to the field. A hysteresis loop also forms in the negative field, the two loops being associated with antiparallel dipoles in adjacent unit-cell sublattices. From the hysteresis loops in Fig. 2, we deduce the critical field to be 9.5 kV/cm for CNO.

4. Discussion

The symmetry considerations of ferroelectricity have been described by Zheludez [14], to which we direct the interested reader for a more thorough treatment. What follows herein is a short summary of these considerations and how they pertain to our experimental results.

Ferroelectric materials must have structures in one of the ten polar point groups, i.e., those with a unique polar axis. These point groups are 1, 2, *m*, *mm*2, 3, 3*m*, 4, 4*mm*, 6, and 6*mm*. Antiferroelectric materials, in contrast, must be in one of the eleven centrosymmetric, nonpolar point groups: −1, 2/*m*, *mmm*, −3, −3*m*, 4/*m*, 4/*mmm*, *m*−3, *m*−3*m*, 6/*m*, and 6/*mmm*. (We also note that while the symmetry considerations are requirements for the respective

ferroelectric properties, they are not sufficient for the property to occur.)

In accordance with the preceding symmetry considerations, the structure for CNO reported in the literature (i.e., in point group *mm*2 and space group *Pnn*2) could be correct if the material were a ferroelectric though not if it were an antiferroelectric. It is therefore crucial to examine the crystallographic evidence as to which point group and space group are correct. We assert that the correct point group is *mmm* and the correct space group is *Pnna*. Our reasons are as follows:

First, the systematic absences from our two data sets are the same as the literature report except that ours also include absences for an a-glide plane, i.e., $h\,k\,0$, $h = 2n+1$. The only space group possible with such a combination is *Pnna* (No. 52) in point group *mmm*.

Second, when we attempted to refine the structure in *Pnn*2, the refinement would not converge and the thermal ellipsoids became non-positive definite. Nonsensical thermal ellipsoids are frequently due to choosing an incorrect space group [15], as we believe was done in the previous structure report.

Third, the literature structure reports tetrahedral Nb–O bond lengths that vary from 1.74 to 1.93 Å while in our structure the same bond lengths are 1.817–1.884 Å, a more narrow distribution. Regular bond lengths and angles are a major factor in the evaluation of the "correctness" of a structure, along with such refinement criteria as residuals and goodness of fit, so the structure reported herein is superior in this regard as well.

Finally, the presence of certain physical properties, such as pyroelectricity or second harmonic generation, are conclusive proofs for certain structural aspects of materials. For example, *lack* of an SHG signal may be due to a very small nonlinear coefficient in a noncentrosymmetric space group rather than the actual presence of a center of symmetry, but the *presence* of an SHG signal is proof for a noncentrosymmetric structure. In the case of CNO, the presence of the antiferroelectric hysteresis requires the structure to be in a nonpolar point group (such as *mmm*) and a space group derived therefrom.

Antiferroelectricity (as well as ferroelectricity) is partially due to long-range interactions between microscopic dipoles created by atomic displacements within the lattice. The crystal structure refinement at high temperature should definitively show what displacements occur at the phase transition, but we have not yet been able to complete such a refinement. We have, however, used group-theoretical means to predict its structure and the atomic displacements that occur upon the transition from the paraelectric to the antiferroelectric phase, which description follows.

To study the origin of the antiferroelectricity, one may deduce the possible high-symmetry (or high-temperature) structure from the low-symmetry structure based on a pseudosymmetry analysis developed by Igartua et al. [16] and implemented by the program PSEUDO at the website www.cryst.ehu.es. When the atomic coordinates of a given structure display an approximate symmetry in addition to the actual space-group symmetry, the structure can be considered as pseudosymmetric with respect to a supergroup containing this additional symmetry. The existence of pseudosymmetry in a crystal structure indicates a slightly distorted structure of higher symmetry. If the distortion is small enough, one can expect the crystal to

Table 4
Predicted high-temperature atomic coordinates of CNO in the *Pnna* basis[a] and the atomic displacements for the phase transition from *Imma* to *Pnna*, cell constants unchanged

Atom	Wyckoff position	x	y	z	Displacements (Å)		
					Δx	Δy	Δz
Cs(1)	8*h*	0.75	0.1924	0.1230	0.0388	0	0
Cs(2)	8*h*	0.75	0.0756	0.3535	0.0164	0	0
Nb(1)	4*e*	0.25	0	0.2312	0	0	0
Nb(2)	4*a*	0.25	0.25	0.25	−0.0739	0	0
Nb(3)	8*h*	0.25	0.1253	0.2613	−0.0336	0	0
Nb(4)	8*g*	0.5	0.0613	0	0.0112	0	0.0189
Nb(5)	8*g*	0.5	0.1883	0.5	0.1225	0	−0.1185
O(1)[b]	16*j*	0.0612	0.1000	0.1333	0.0026	−0.0058	0.0026
O(2)[b]	16*j*	0.0644	0.1367	0.3770	0.0045	0.0043	0.0089
O(3)[b]	16*j*	0.0640	0.2338	0.3738	0.0037	−0.0072	0.0115
O(4)	8*h*	0.25	0.0517	0.3298	−0.0052	0	0
O(5)	8*h*	0.25	0.1844	0.1859	−0.0142	0	0
O(6)	8*i*	0.4525	0	0.1241	0	0.0058	0
O(7)[b]	16*j*	0.4389	0.1000	0.1333	0.0026	0.0058	−0.0026
O(8)[b]	16*j*	0.4356	0.1367	0.3770	0.0045	−0.0043	−0.0089
O(9)[b]	16*j*	0.4360	0.2338	0.3738	0.0037	0.0072	−0.0115
O(10)	8*h*	0.75	0.0529	0.0514	0.0060	0	0
O(11)	8*h*	0.75	0.1854	0.4352	0.0217	0	0

[a]The coordinates of atoms in *Pnna* and Imma basis are related by an origin shift of $(\frac{1}{4}, \frac{1}{4}, \frac{1}{4})$.
[b]O(1) and O(7), O(2) and O(8), and O(3) and O(9) are equivalent in *Imma*, respectively.

acquire this higher symmetry at a higher temperature. The analysis searches for pseudosymmetry in a given structure among the minimal supergroups of the structure's space group, thus predicting possible phase transitions.

Using the space group, lattice parameters, and atomic coordinates of the 100-K structure, we performed a pseudosymmetry search among all the minimal supergroups of *Pnna*. The maximum atomic displacement was restricted to 0.75 Å. Of the minimal supergroups of *Pnna*, we determined Imma (no. 74) was the only pseudosymmetric minimal supergroup that would produce a maximum atomic displacement of 0.17 Å. We therefore concluded the high-temperature paraelectric phase of CNO is in this space group. The predicted atomic coordinates are listed in Table 4 along with the atomic displacements along each axis for the phase transition from *Imma* to *Pnna*. In the calculation, we neglected changes in volume and other symmetry-preserving distortions that could occur at the phase transition.

In a crystal that consists of polyhedra of oxygen atoms in its lattice, a displacive phase transition is usually caused by displacements of cations within the polyhedra. In the present study, we observed antiferroelectricity only along the *c*-axis, which means the antiparallel displacements of the atoms are parallel to this axis. Examination of Table 4 shows that the only cations with displacement components in the *c*-axis are Nb(4) and Nb(5), which occupy Wyckoff position 8(g) in *Imma*. During the phase transition, based on the pseudosymmetry analysis, half of these niobium atoms shift in one direction along the *c*-axis and half shift in the opposite direction—see Fig. 3. The oxygen atoms that form the $Nb(4)O_6$ and $Nb(5)O_6$ octahedra (O(1)–O(3) and O(7)–O(9), respectively) also have *c*-axis displacements. We therefore conclude the antiferroelectricity in CNO originates from the distortions of the $Nb(4)O_6$ and $Nb(5)O_6$ octahedra and the displacements of the niobium atoms contained therein, with a majority contribution from the latter because Nb(5) has the largest displacement.

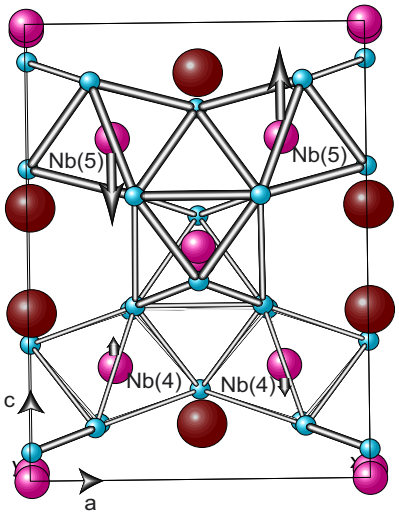

Fig. 3. Projection of the predicted *Imma* structure of CNO along the *b*-axis. Arrows indicate the antiparallel shifts of Nb(4) and Nb(5) along the *c*-axis.

The study of antiferroelectricity in solid materials is fairly sparse, and the number of reported solid-state antiferroelectrics few, although antiferroelectricity in liquid crystals is a field of growing interest because of their ability to switch rapidly between three stable states in optical displays [17]. Some examples of solid-state antiferroelectric materials studied recently include $Sr_9In(PO_4)_7$ [18], BaFCl [19], and $PbZrO_3$ [20], the last of which has been studied extensively, along with solid solutions pertaining thereto. CNO is thus a noteworthy addition to the field of study.

Acknowledgments

We thank Professor Kharitonova of Moscow State University for the single crystal and Professor Alexander of University of Nebraska—Lincoln for assistance with the SHG experiment. This work was supported by the Nebraska Research Initiative.

References

[1] A. Reisman, J. Mineo, J. Phys. Chem. 65 (1961) 996–998.
[2] M. Gasperin, Acta Crystallogr., Sect. B 37 (1981) 641–643.
[3] E.P. Kharitonova, V.I. Voronkova, V.K. Yanovskii, S.Y. Stefanovich, J. Cryst. Growth 237–239 (2002) 703–706.
[4] Y. Miseki, H. Kato, A. Kudo, Chem. Lett. 34 (2005) 54–55.
[5] J. Liu, E.P. Kharitonova, C.-G. Duan, R.W. Smith, J.R. Hardy, J. Chem. Phys. 122 (2005) 144503.
[6] R. Schelkens, Phys. Stat. Sol. 37 (1970) 739–743.
[7] SMART (version 6.532), Program for Bruker CCD X-ray Diffractometer Control, Bruker AXS, Inc., Madison, WI, 2005.
[8] SAINT+(version 6.45), Program for Reduction of Data Collected on Bruker CCD Area Detector Data, Bruker AXS, Inc., Madison, WI, 2003.
[9] G.M. Sheldrick, SADABS, (version 2.10), Program for Empirical Absorption Correction of Area Detector Data, University of Göttingen, 2003.
[10] G.M. Sheldrick, SHELXTL (version 6.14), Program Package for Structure Solution and Refinement, Bruker AXS, Inc., Madison, WI, 2000.
[11] R.D. Shannon, Acta Crystallogr., Sect. A 32 (1976) 751–767.
[12] S. Tsunekawa, T. Kamiyama, K. Sasaki, H. Asano, T. Fukuda, Acta Cryst., Sect. A 49 (1993) 595–600.
[13] M.E. Lines, A.M. Glass, Principles and Applications of Ferroelectrics and Related Materials, Clarendeon Press, Oxford, 1977.
[14] I.S. Zheludev, in: H. Ehrenreich, F. Seitz, D. Turnbull (Eds.), Solid State Physics Advances in Research and Applications, vol. 26, Academic Press, New York, 1971, p. 429.
[15] R.L. Harlow, J. Res. Natl. Inst. Stand. Technol. 101 (1996) 327–339.
[16] J.M. Igartua, M.I. Aroyo, J.M. Pérez-Mato, Phys. Rev. B 54 (1996) 12744–12752.
[17] J.M. Oton, X. Quintana, P.L. Castillo, A. Lara, V. Urruchi, N. Bennis, Opto-Electron. Rev. 12 (2004) 263–269.
[18] S. Yu. Stefanovich, A.A. Belik, M. Azuma, M. Takano, O.V. Baryshnikova, V.A. Morozov, B.I. Lazoryak, O.I. Lebedev, G. Van Tendeloo, Phys. Rev. B 70 (2004) 172103.
[19] B. Sundarakkannan, R. Kesavamoorthy, J. Adelene Nisha, V. Sridharan, T. Sivakumar, Phys. Rev. B 57 (1998) 11632–11638.
[20] E. Buixaderas, S. Kamba, J. Petzeit, Ferroelectrics 308 (2004) 131–192.